Supplementary Information

Dynamics of cell size and force during *spreading*

Yifat Brill-Karniely[1], Noam Nisenholz[1], Kavitha Rajendran[2], Quynh Dang[2], Ramaswamy Krishnan[2], and Assaf Zemel[1],*

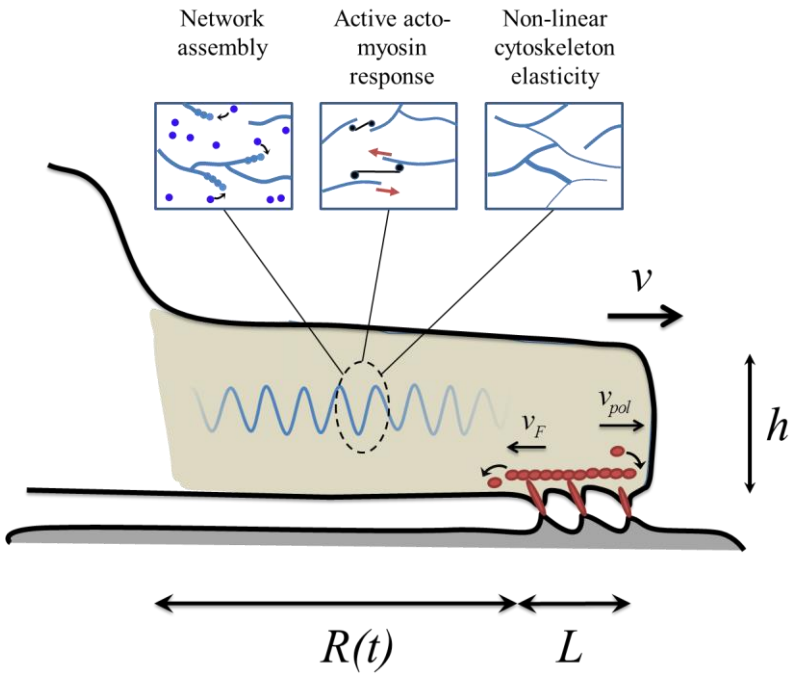

Figure S1: Schematic illustration of major elements of the model. The cell is modeled as a circular disc of radius *R(t)* and thickness *h* that is adhered to the substrate along a narrow rim, $L \ll R(t)$ that is assumed to be constant during spreading. Actin polymerization (red circles) at the cell front provides the driving force for cell spreading. Experiments suggest that the radial polymerization speed, v_{pol}, is constant during spreading. In contrast, the retrograde flow, $v_F(t)$, increases in the course of spreading while the radial extension speed, $v(t) = dR(t)/dt$, decelerates with time (1). This is explained here by the rise in elastic tension in the cytoskeleton. The shaded spring in the cell center is there to represent the underlying viscoelastic response of the cell (including the cytoskeleton and the membrane). Three models are presented to account for the non-linear coupling between cell size and force during spreading; those are shown with the three cartoons above. Left, middle and right panels illustrates the network assembly model, actomyosin polarization model and the non-linear elastic model, respectively.

1. Materials and Methods

Combined, time-resolved force and area measurements in cultured human pulmonary artery endothelial cells (HPAECs)

Preparation of gel-substrates: Cells (Lonza,cat#CC-2530) were detached with 0.25% Trypsin- EDTA (1x) (Life Technologies, cat #25200-056) from a standard cell culture flask and re-suspended in growth medium (EGM2 bulletkits, cat # CC-3162, Lonza Inc.) supplemented with 10% fetal bovine serum (cat#45000-736, VWR International). The medium containing cells was then added to the surface of 26kPa stiff polyacrylamide gel substrates. The substrates were prepared within 35mm glass bottom dishes (Mattek, USA) as has been previously described (2) with a few modifications. Briefly, a small volume of an acrylamide-Bisacrylamide mixture was dissolved in ultrapure water containing 7.5% acylamide, 0.3% Bisacrylamide, 0.5% ammonia persulfate, and 0.05% TEMED (Bio-Rad, Hercules, CA) and polymerized between glass coverslips to yield gels that were ~100 μm thick. The polymerized gel surfaces were activated using Sulfosuccinimidyl-6-[4-azido-2-nitrophenylamino] hexanoate (Sulfo-SANPAH; Pierce, Rockford, IL) and conjugated with sulfate-modified fluorescent latex nanospheres (diameter = 200 nm, F8848, Life Technologies) by delivering a bead suspension on top of the gels for 20 minutes (3). The bead solution was carefully removed to discard any suspended or unattached beads, replaced with type I Collagen dissolved in PBS solution (0.1 mg/ml; cat#5505-B, Advanced Biomatrix) and stored overnight at 4°C. The bead binding step was repeated on the following day. The gels were then washed, hydrated with PBS, and stored at 4°C until the day of the experiment.

Cell-spreading measurements: All measurements were performed in a microscope chamber (37^0C and 5% CO2) using an inverted fluorescence microscope (DMI 6000B, Leica Inc). Phase contrast images of cells were obtained together with fluorescent images of nanospheres. From the phase contrast images, by manually tracing cell contours, we calculated the cell spreading area. From the fluorescent nanosphere images, by comparing images during cell spreading with the same region of the gel after cell detachment from the substrate, we calculated the cell-exerted displacement field. The displacements were calculated through cross-correlation using

the fast fourier transform method in Matlab. From knowledge of the displacement field together with the previously determined gel elastic modulus (26 kPa), we computed the cell-generated forces by solving the inverse Boussinesq solution using the well-established procedure of Fourier transform traction microscopy (2). During its implementation, we minimized any experimental artifacts that may have arisen during the measurements of displacements through the constrained traction method, where tractions outside the boundary of the cell are set to be zero. From the traction map, we calculated total force over the cell, *F*, by summing the absolute magnitude. Next, we determined the traction density as $f=F/(2\pi R)$. These calculations were performed from experimental measurements obtained every five minutes for the total duration of approximately an hour.

2. **Effect of cell volume on spreading dynamics**

It is generally expected that cells of larger volume and larger cytoskeleton mass would show a longer period in which the assembly of the cytoskeleton network at the cell basis accompanies spreading. According to our elastic picture, this process changes the effective "rest-length'' of the cytoskeleton and therefore modulates the dynamics of force generation during spreading. To the best of our knowledge, it is unknown how *cell volume* alters the dynamics and mechanics of spreading. Thus, in this section we examine this issue theoretically. In comparing cells of different volumes we assume that the concentration of suspended cytoskeletal material, c(0), is fixed. In addition, the initial projected cell radius, $R(0)$, is assumed to scale with the cell volume and to be equal to the stress-free radius, $R_0(0)$, such that in the onset of spreading, $R(0) = R_0(0) = \beta V^{1/3}$; where β is a proportionality constant that can be obtained by the fit to experimental data. Eqs. 4 and 5 provide a simple kinetic model for the growth-dynamics of the stress-free area of the lamellar cytoskeleton $A_0(t) = \pi R_0^2(t)$ at the cell basis. Accordingly, the larger the cell volume, and consequently also A_0, the faster is the assembly rate since the number of available binding sites is larger. As a result, the cell may spread by assembling the lamellar cytoskeleton, and yet without generating elastic stresses in the cytoskeleton. This is shown for example by the red curves in Fig. S2. Panels a. and b. show the evolution of cell radius and

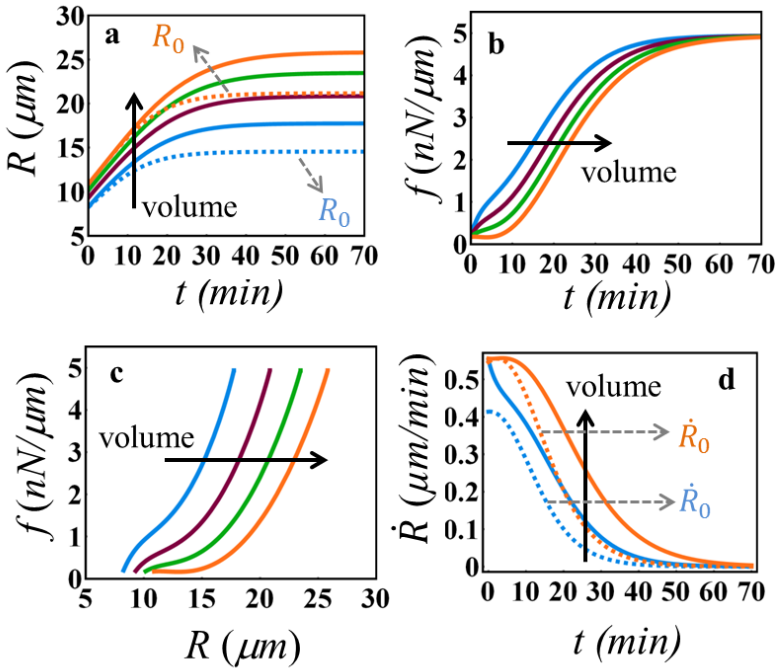

Figure S2: Effects of cell volume on spreading dynamics and mechanics. Panels a and b exhibit the evolution of cell radius and force respectively. Dashed lines in (a) is the stress-free radius as calculated analytically from Eqs. 4 and 5. Panel c. shows a parametric plot of the radial cell force as a function of cell radius. Panel (d) presents the radial spreading speed, $\dot{R}(t)$, along with the radial assembly speed, $\dot{R}_0(t)$ for the largest (orange) and smallest (light blue) cells. Parameters used in the calculation are: *V* (μm^3)=*2200* (light blue), *3150* (purple), *4100* (green), *5050* (orange), *h=1 μm*, $\rho=1.1\cdot10^7$ *molec/μm*^{2}, *c(0)=3.8 mM*, v_{pol}*=0.58 μm/min*, κ_c*=11* kPa, ξ_c*=1.67* kPa·*min*, ξ_s *=8.4* kPa·*min*, δ*=26.4 (M·min)*$^{-1}$.

force, respectively. So long as the radial assembly speed is equal to the spreading velocity, $v = \dot{R} \approx \dot{R}_0$, no tension is developed in the cell. The elastic phase begins once the available suspended material for lamellar assembly diminishes and consequently further spreading is associated with stress generation.

In cells of smaller volume (e.g., light blue), the assembly rate is slower due to the smaller number of binding sites on the smaller 2D network area. However, because the polymerization speed, v_{pol}, is likely to be similar (since it is dictated by similar G-actin concentration), the spreading speed $v = \dot{R}$ can exceed the assembly-growth speed $\dot{R}_0$ and as a result the cell may develop tension already at early-times. The comparison between $\dot{R}_0(t)$ and $\dot{R}(t)$ is shown in panel (d) for two cells that only differ in volume. While for both cell cases, $\dot{R}(0) \approx v_{pol}$ since no elastic tension has yet been generated (and the viscous force is relatively small), $\dot{R}_0(t)$ is lower for the

smaller cell and consequently stresses develop more quickly in the onset of spreading. The effects of these different dynamics on the $f(t)$ versus $R(t)$ curve is shown in panel c. The apparent non-linearity of $f(R)$ is seen to be more pronounced the larger the cell is.

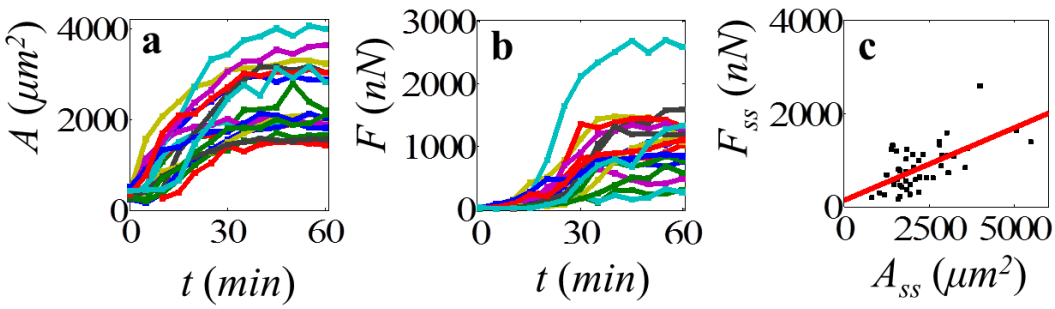

Figure S3: Evolution of cell area and total force during spreading. Panels a. and b. show the respective spreading data for 18 representative cells in our collection. Panel c. is a scatter plot of the *steady-state* force and area, collecting the end-points from our entire collection of cells (47 cells). Red line is a linear fit (slope=0.31 kPa, R^2=0.4).

3. Data for total cell force and area

Fig. S3 shows measured data of the evolution of cell area, $A(t)$, and total cell force, $F(t)$, for individual cells in our collection. These are related to the temporal traction density, f, and cell radius via: $F \approx 2\pi R\, f$ and $A \approx \pi R^2$. Panel c. provides a scatter plot of the steady-state force, F_{ss} as function of the steady-state area of cells, A_{ss}. The seemingly linear dependence between F_{ss} and A_{ss} suggests that also f_{ss}~R_{ss}; yet note the small R^2 value. Manipulating the data to plot f_{ss} as function of R_{ss}directly, increases the relative noise and the corresponding R^2 value reduces to 0.06. Nevertheless, we note the apparent difference in the behavior of the steady-state dependence of F_{ss} on A_{ss}, Fig. S3.c, and the profound non-linear dependence of the temporal force $f(t)$ on $R(t)$, shown in Fig.1c. A linear dependence of F_{ss} on A_{ss} may indicate that the cytoskeleton behaves in a linear fashion during spreading and the apparent non-linearity of the $f(R)$ curve would then be explained by the different dynamics of cell area and force as explained with models (i) and (ii) in the manuscript. Nevertheless, since the R^2=0.4 is rather low in panel c. we are unable to reach any conclusion about this issue in the current manuscript.

Table S1. Parameters used in Figure 1.

Parameter	Notation	Network assembly	Actomyosin polarization	Non-linear	Refs (in SI)
Initial lamella radius*	*R(0) (μm)*	11.2	10.3	10.8	-
Average lamella height	*h (μm)*	1.7	1	1	4,5
Cell volume	*V (μm^3)*	4500	-	-	-
Surface density of lamellar network	*ρ (molec/μm^2)*	$1.85 \cdot 10^7$	-	-	6
Assembly rate constant	*δ (M·min)$^{-1}$*	9.96	-	-	-
Initial concentration of suspended cytoskeleton constituents (based on actin)	*c(0) (mM)*	9.2	-	-	6
Radial actin polymerization speed	*v_{pol} (μm/min)*	0.59	0.68	0.63	1
Effective cytoskeletal rigidity	*κ_c (*kPa*)*	10	0.07	0.13	8
Lamella viscosity coefficient	*ξ_c (*kPa·*min)*	1	0.07	3.58	9
Cell-substrate friction coefficient	*ξ_s (nN·min/μm^2)*	8.3	6.4	7.2	-
Stress-stiffening factor	*λ*	-	-	2.75	7
Actomyosin susceptibility	*α*	-	22	-	-
Actomyosin polarization response time	*τ_p (min)*	-	15	-	-

* $R(0) = R_0$ in the polarization and non-linear models and $R(0) = R_0(0)$ in the assembly model.

4. Data Fitting in Figure 1

Table S1 lists the parameters obtained from fitting the three models to our experimental data. The right most column provides references (listed at the bottom of this document) for comparison for few of the fitted parameters. The order of magnitude of the phenomenological surface density parameter, ρ, and initial concentration of suspended constituents, *c(0)* is consistent with the size ($v = h/\rho \sim 10^{-7}\mu m^3$) and bulk-concentration of actin monomers (Ref. 6) which is the main polymer in the lamellar network. The cytoskeleton viscosity, $\xi_c = 1\ kPa\ min$ is

estimated based on the measurements in Ref. 9 below. Since the number of fitting parameters is large, (between 6-7) and more importantly, since it is very likely that the three mechanisms operate simultaneously the values we obtain by these fits *should not* be considered as quantitative estimates of these parameters. Rather, the purpose of the fits shown in Fig.1 is to demonstrate that all three models may separately capture the *qualitative* behavior of cell size and force during spreading and hence to contribute to the observed phenomena.

5. Comments and parameters for Fig. 2

Fig. 2 highlights the difference between the temporal dependence of $f(t)$ on $R(t)$ (solid lines) and the corresponding dependency of the steady-state values of f_{ss} and R_{ss} (dashed lines). While the relation between $f(t)$ and $R(t)$ reflects the various dynamical processes that take place in the cytoskeleton during spreading (such as network assembly and actomyosin polarization), the dependence of f_{ss} on R_{ss} (and equivalently of F_{ss} on A_{ss}, Fig. S2) reflects the underlying (passive) constitutive relation of the cytoskeleton. Different curves were plotted for various values of the substrate rigidity. A relatively high viscosity constant, ξ_c *=45* kPa·min was used in order to visually separate the different curves; this also required adjustment of the network assembly rate constant, δ, to keep the early-time force comparable to the two other models. The values of κ_c were adjusted in the three models to obtain the same level of overall strain $(R_{ss} - R_0)/R_0$ since both the acto-myosin polarization model and the nonlinear elasticity model possess different stiffening mechanisms of the cytoskeleton, one via the polarizability factor, $\propto$, the other via the stiffening factor λ. Finally, throughout, we used $P_0 = 0$ implying that $P(t) - P_0 = P(t)$ measures the strengthening of the acto-myosin dipolar stress. The basal level of myosin contraction is then implicitly represented in the value of the cytoskeleton rigidity, κ_c. The parameters used in Fig. 2 are listed in Table S2.

Table S2. Parameters used in Figure 2

Parameter	Notation	Network assembly	Actomyosin polarization	Non-linear
Initial lamella radius*	$R(0)\ (\mu m)$	10	10	10
Average lamella height	$h\ (\mu m)$	1	1	1
Cell volume	$V\ (\mu m^3)$	4500	-	-
Surface density of lamellar network	$\rho\ (molec/\mu m^2)$	$1.85 \cdot 10^7$	-	-
Assembly rate constant	$\delta\ (M \cdot min)^{-1}$	55.8	-	-
Initial concentration of suspended cytoskeleton constituents (based on actin)	$c(0)\ (mM)$	9.3	-	-
Radial actin polymerization speed	$v_{pol}\ (\mu m/min)$	0.8	0.8	0.8
Effective cytoskeletal rigidity	κ_c (kPa)	10	1.4	1.9
Lamella viscosity coefficient	ξ_c (kPa·min)	45	45	45
Cell-substrate friction coefficient	$\xi_s^{max}\ (nN \cdot min/\mu m^2)$	10	10	10
Stress-stiffening factor	λ	-	-	2.75
Acto-myosin susceptibility	α	-	3	-
Actomyosin polarization response time	$\tau_p\ (min)$	-	2	-

6. References

1. Giannone, G., B. J. Dubin-Thaler, H.-G. D¨obereiner, N. Kieffer, A. R. Bresnick, and M. P. Sheetz, 2004. Periodic lamellipodial contractions correlate with rearward actin waves. *Cell* 116:431–43.
2. Butler, J. P., Toli´c-Nørrelykke, I. M., Fabry, B. & Fredberg, J. J. Traction fields, moments, and strain energy that cells exerton their surroundings. *American Journal of Physiology-Cell Physiology* 282, C595–C605 (2002).
3. Marinković, A., Mih, J. D., Park, J. A., Liu, F., & Tschumperlin, D. J. (2012). Improved throughput traction microscopy reveals pivotal role for matrix stiffnes in fibroblast contractility and TGF-β responsiveness. *American Journal of Physiology-Lung Cellular and Molecular Physiology*, *303*(3), L169-L180.
4. Pang, K. M., E. Lee, and D. a. Knecht, 1998. Use of a fusion protein between GFP and an actin-binding domain to visualize transient filamentous-actin structures. *Curr. Biol.* 8:405–8.
5. Fardin, M., O. Rossier, P. Rangamani, P. Avigan, N. Gauthier, W. Vonnegut, A. Mathur, J. Hone, R. Iyengar, and M. Sheetz, 2010. Cell spreading as a hydrodynamic process. *Soft Matt.* 6:4788–4799.
6. Lodish, H., Berk, A., Kaiser, CA., Krieger, M., Scott, MP., Bretcher, A., Ploech, H. and Matsudaira, P, 2012. Molecular Cell Biology 7th edition, Macmillan Higher Education, Aug 1, 2012 - Science.
7. Kollmannsberger, P., Mierke, C. T. & Fabry, B. Nonlinear viscoelasticity of adherent cells is controlled by cytoskeletal tension.*Soft Matter* 7, 3127–3132 (2011).
8. Rodriguez, Marita L., Patrick J. McGarry, and Nathan J. Sniadecki. "Review on cell mechanics: experimental and modeling approaches." Applied Mechanics Reviews 65.6 (2013): 060801.
9. Bausch, Andreas R., Winfried Möller, and Erich Sackmann. "Measurement of local viscoelasticity and forces in living cells by magnetic tweezers." Biophysical journal 76.1 (1999): 573-579.